

Analysis of the Photothermal Engine Cycle in an AFM-IR Measurement of Photothermal Expansion

Luca Quaroni

Department of Physical Chemistry and Electrochemistry, Faculty of Chemistry, Jagiellonian University, 30-387, Kraków, Poland

e-mail: luca.quaroni@uj.edu.pl

Keywords: Photothermal effect; AFM-IR; micro engine; infrared spectroscopy; optomechanical sensor; scanning probe

Abstract

We develop a thermodynamic description of signal generation in micromechanical measurements of the photothermal effect. Photothermal expansion can be measured with high spatial resolution via a mechanical detection scheme that relies on deflection of a cantilevered probe for atomic force microscopy. The response relies on the complex interplay of multiple factors, including optical, thermal, and mechanical properties of both sample and probe. In the present work we provide a new framework to analyze the thermomechanical processes that underlie signal generation in terms of a thermodynamic engine cycle. We discuss the general properties of this photothermal micromechanical engine, considering two forms of light excitation, progressive and impulsive, and we derive guidelines for performance optimization of the photothermal measurement. We observe that the engine is intrinsically inefficient because most or all the energy derived from light absorption is dispersed to the environment as heat. Nonetheless, we also argue that efficiency is not the core parameter when considered in the context of the main purpose of this mechanism, which is analytical, as opposed to the conversion of heat into work. We discuss two forms of excitation, gradual and impulsive. For the case of gradual excitation, we derive a simple analytical relationship to assess the dependence of signal intensity from the thermomechanical properties of sample and probe, and we use it to obtain guidelines for the optimization of photothermal micromechanical experiments.

1.0 Introduction

The photothermal effect converts light absorbed by a material into heat, leading to a temperature increase and to expansion. Photothermal expansion is wavelength dependent and tracks the absorption coefficient of the material, making it a useful probe of the spectroscopic properties of a sample. Among the multiple measurement configurations, the use of atomic force microscopy (AFM) instrumentation to detect photothermal expansion is receiving increasing attention. The configuration measures expansion via the deflection of the cantilever of an AFM probe in contact with the sample.[1] The spatial resolution of the measurement does not depend on the wavelength of absorbed light, but on the interplay of tip size and the size of the thermal expansion volume.[2] Interest in the technique is driven by the possibility of spectroscopic analysis with resolution beyond the optical diffraction limit.[3] This is particularly valuable in the extensively used mid-infrared (mid-IR) spectral region, because of the relatively long wavelength ($\lambda \sim 2.5 - 25 \mu\text{m}$). Delivery on such promise can extend the impact of mid-IR absorption spectroscopy to nanoscale samples, a development of great interest to both academic and industrial researchers. The detection of

photothermal expansion with mid-IR light using the deflection of an AFM cantilever was first performed by Anderson using conventional benchtop instrumentation.[1] These preliminary experiments demonstrated a measurable cantilever deflection driven by photothermal expansion. They also provided a mechanically-detected interferogram from the scanning operation of the Michelson interferometer. However, the signal-to-noise ratio was not sufficient to deliver an absorption spectrum from the Fourier-Transform of the interferogram. The method was later developed into a technique for spectroscopic analysis using the pulsed emission from a Free-Electron laser as a light source.[4] The commercial development of the AFM-IR detection scheme with benchtop laser sources has further widened its appeal and its accessibility to a larger pool of researchers. While the first demonstration of AFM-IR detection was carried out using continuous wave (CW) light sources, it is currently implemented mostly with pulsed laser sources. Different names are used to describe the various incarnations of photothermal measurements with AFM detection, of which the most common ones are AFM-IR [4] and Photothermal Induced Resonance (PTIR) [5]. The former has seen more general use, while the latter is restricted to the case of impulsive excitation. In the present work, AFM-IR will be the main moniker, encompassing all configurations.

The technique is seeing increased popularity and a general drive towards wider applications in multiple fields. However, popularization of the technique has come at the cost of neglecting investigations of the underlying signal generation mechanism. The possibility to relate the absorption spectrum obtained from photothermal measurements to its far-field equivalent relies on having a detailed understanding of the physical processes involved in signal generation and how they relate to the absorption coefficient of the sample. However, some fundamental aspects of AFM-IR remain unclear, and experimental observations are not properly addressed by existing theoretical models. The shortcoming arises from the complexity of the micromechanical signal transduction mechanism, which relies on the interplay of spectroscopic, thermal, and mechanical properties of the sample. It is the purpose of the present analysis to expand the theoretical modelling of such mechanism.

It is already appreciated that the scanning probe detection mechanism introduces a dependence of the signal from the mechanical properties of tip-sample interaction.[6][7][8][9][10] A less studied aspect is the role of heat-transfer processes on signal generation. This facet has been addressed using Fourier's heat transfer theory,[6][11] but a systematic thermodynamic treatment is still missing. In thermodynamic terms, measurements such as those of an AFM-IR experiment rely on a microscopic engine, a device that converts heat into work. Energy from absorbed photons heats the sample which, by expanding, delivers the work necessary to deflect the cantilever of the AFM probe. In the following sections we will assess the merits of this model in describing photothermal experiments with micromechanical detection.

The analysis will be developed in four main sections. The first section will lay the general concepts in the analysis of a micromechanical photothermal engine. The second section will address the specific case of gradual excitation, whereby the deflecting AFM probe retains contact with the photothermal expansion zone. A quantitative description of signal generation will be proposed for this mechanism. The third section will discuss the case of excitation by a pulsed light source, whereby the rapid expansion and contraction of the sample drives the oscillation of multiple modes of the cantilever. Because of the complexity of impulsive excitation and the multiple interactions involved in the process, beyond simple photothermal

displacement, only a qualitative discussion will be provided of the latter. A fourth section will discuss the possibility to verify the conclusions of the previous sections.

2.0 Analysis and Discussion

2.1 The Micromechanical Detection Scheme of Photothermal Expansion is Described as a Photothermal Engine.

A graphical representation of the basic micromechanical detection scheme is shown in Figure 1A. A cantilevered probe measures light absorption via the expansion of the absorbing region. The sample is mounted as for a conventional AFM experiment and irradiation occurs by focusing light at the tip-sample contact region. An absorbing sample expands upon illumination and the expansion is recorded via the deflection of the cantilever and quantified by the movement of the AFM monitor laser on a four-quadrant detector, as in conventional AFM. The deflection is generally assumed to be proportional to the local absorption coefficient of the sample at the wavelength of irradiation and is used for spectroscopic analysis.[12] Photothermal measurements can be carried out as both spectromicroscopy and imaging experiments. In the former, the probe is kept stationary while the light source is scanned through the spectral range of interest. In the imaging configuration the AFM tip is scanned over the sample while the light source is modulated or pulsed at a single wavelength. A multiplexing approach, whereby a broadband light source excites the sample and is analyzed by a Michelson interferometer, is also possible.[1,13,14]

The analysis of the AFM-IR experiment relies on the definition of an engine cycle that best describes the processes occurring during turnover. The first step is the ideal breakdown of the measurement into the separate stages or strokes of a cyclic process, as shown in Figure 1B. The sample is the working medium of the engine, and the two terms will be used interchangeably in this work. In contrast to common, macroscopic heat engines, the working medium is solid. The initial state (State 1) is described by a set of thermodynamic variables, pressure (P), volume (V) and temperature (T). In the first stroke, light absorption delivers energy to the medium, simultaneously increasing both T and P, and bringing it to state 2. In the second stroke, the sample expands, reaching State 3. In the transition from State 2 to State 3, expansion acts against the force exerted by the cantilever and causes its deflection. In the third stroke, the expanded sample cools down (thermalizes) to the initial temperature, typically room temperature, leading to State 4. In the fourth and last stroke, the cooled (thermalized) sample, is compressed back to its initial volume, corresponding to the initial state. In the most general case, the sequence of steps is schematically represented in Figure 1C as an ideal cycle in the PV plane (black line).

We assume that the engine operates between two temperatures T_1 and T_2 , with $T_1 < T_2$, corresponding to respective heat reservoirs. If the expansion and compression strokes are isothermal transformations, then $T_2 = T_3$ and $T_4 = T_1$. Energy is absorbed as photons during stroke 1 – 2 and is here represented as an equivalent heat input ($Q_{in} \equiv hv$) and raises the temperature of the medium to T_2 , corresponding to the higher energy reservoir. During stroke 3 – 4, heat is released to the environment (Q_{out}), which acts as the low temperature heat reservoir at temperature T_1 . Additional heat exchange can also take place during the expansion stage 2 - 3 (Q_{in}) and the compression stage 4 - 1 (Q_{out}). Expansion work (W_{out}) is executed by the medium on the cantilever during stroke 2 – 3 and is executed by the cantilever on the medium (W_{in}) during compression. As in heat engines, the area of the cycle

in Figure 1C provides the total work executed by the engine on the environment ($W_{\text{tot}} = W_{\text{out}} - W_{\text{in}}$) and the efficiency of the engine ($\eta = W_{\text{tot}}/Q_{\text{in}}$). The individual identity of the strokes is a conceptual abstraction, valid for quasi-static transformations, and is lost in a real cycle, which would resemble a distorted ellipsoid (dotted red line).

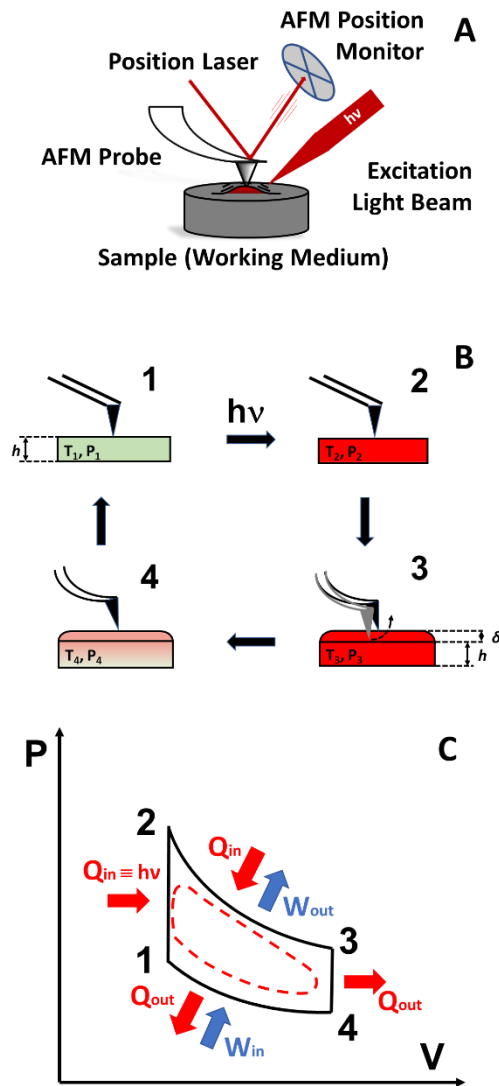


Figure 1. Photothermal signal generation as an engine cycle. **A.** AFM detection of photothermal expansion. **B.** States of the engine and transformations. T_n , P_n , V_n : respectively, temperature, pressure and volume of state n . d : sample thickness. δ : cantilever deflection. **1.** Initial state. **2.** After temperature increase following light absorption. **3.** After expansion from state **2**. **4.** After thermalization of state **3**. Red color graphically indicates higher temperature. In the case of isothermal expansion and compression, $T_2 = T_3$ and $T_4 = T_1$. In the case of isochoric heating and cooling, $V_1 = V_2$ and $V_3 = V_4$. **C.** The photothermal micromechanical engine cycle. Numbering of cycle states corresponds to the states of Figure 1A. The solid lines represent the quasi-static transformations corresponding to the strokes of the cycle, following the numbering in panel B. The dotted red line represents the overall transformation in the case of a real cycle, where quasi-static conditions are not met.

As in the analysis of conventional cycles, the cycle represented in Figure 1 implies quasi-static operation. For finite evolution times, expansion and contraction of the working medium are far from ideal, since cooling of the sample occurs rapidly and continuously during both stages. Heat dissipation takes place at multiple interfaces, including the sample-substrate, sample-tip, and sample-air interfaces, plus any interfaces between sample phases. The effect of the resulting real PV cycle on performance parameters is graphically represented in Figure 2. Faster heat dissipation under non-thermostatic conditions leads to a smaller area of the cycle and eventual reduction to a three-stroke cycle. In turn this corresponds to decreased W_{tot} , lower efficiency, lower maximum expansion volume of the medium ($V''_{max} < V'_{max} < V_{max}$) and lower deflection ($\delta''_{max} < \delta'_{max} < \delta_{max}$), with a consequently weaker AFM-IR signal.

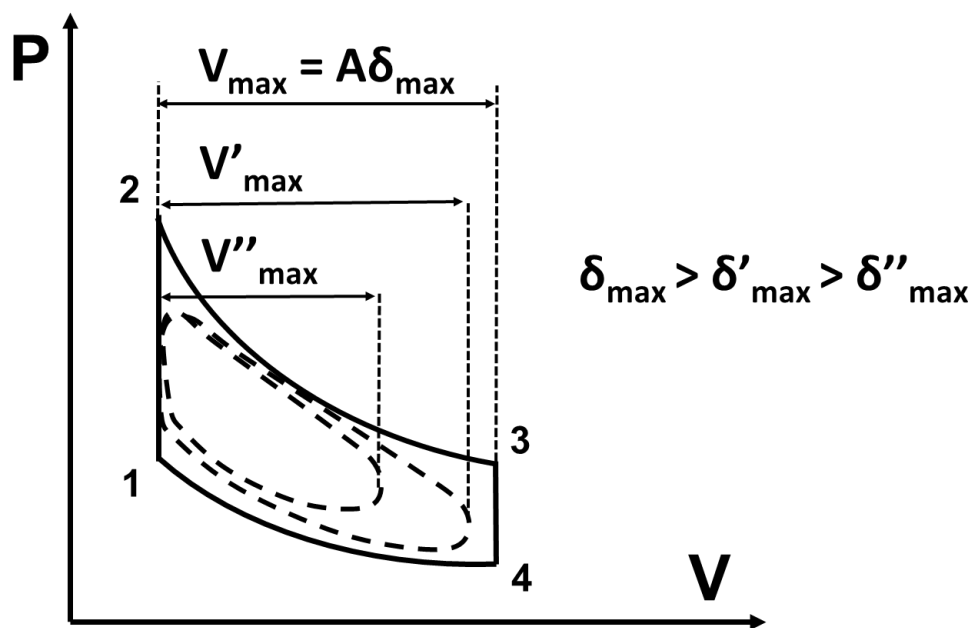


Figure 2. Comparison of ideal and real PV cycles of a photothermal engine. Deviation from the ideal cycle (solid line) is assumed to be mostly from the breakdown of thermostatic conditions during expansion and contraction stages. The resultant cycles (dotted lines) provide reduced expansion, which corresponds to lower maximum expansion volumes ($V''_{max} < V'_{max} < V_{max}$) and reduced deflection of the cantilever ($\delta''_{max} < \delta'_{max} < \delta_{max}$).

It is desirable to design the engine cycle to correct for these factors. It can be inferred from Figure 2 that achieving thermostatic conditions during expansion and compression as well as synchronizing heat dissipation with maximum expansion can bring the cycle closer to its ideal counterpart. In turn, these conditions will deliver larger expansion and increased AFM-IR signal, as discussed in the following sections for the two experimental configurations currently in use for AFM-IR measurements, with gradual excitation or impulsive excitation.

2.2 Case 1: Spring-Loaded Engine with Gradual Excitation.

One class of AFM-IR experiments involves the use of non-impulsive light sources for photothermal excitation. In such a design, the sample is irradiated with a continuous wave

(CW) laser or a thermal source which are slowly (approx. 0.1 – 10 Hz) modulated in intensity. Historically, this was the configuration used for the first demonstrations of the AFM-IR principle. In the case of monochromatic or narrow band excitation, the beam is modulated by a chopper. In the case of broadband excitation, it is modulated by scanning the optical path difference of an interferometer.[1,13] Irradiation causes a progressive increase of temperature in the medium, until illumination is interrupted or decreased and the sample is allowed to cool down. In both cases, the deflection of the cantilever tracks the slow expansion and contraction of the sample, without loss of contact. Both modes of operation will be here described as *gradual excitation*. It is notable that a configuration using interferometric light modulation, described by Donaldson *et al.*[14], relies on the use of a synchrotron light source. The synchrotron emission is pulsed at such high frequency compared to the response time of conventional infrared detectors that it is generally considered to be a continuous source in optical experiments, although the validity of such assumption has not been confirmed for photothermal experiments.

Under conditions of gradual excitation, heating and expansion can be considered to occur simultaneously, providing a substantially different and simpler cycle compared to the general one shown in Figure 1. Strokes 1 – 2 and 2 – 3 from Figure 1 can be represented as a single transformation, extending between the two isotherms that represent the thermal reservoirs at T_1 and T_2 (Figure 3, Stroke 1 – 2). Similarly cooling and compression are simultaneous and can be represented as the reverse path in a PV diagram (stroke 2 – 1 in Figure 3).

The harmonic response of the cantilever sets this mechanism apart from that of most conventional heat engines. Work output from the expanding medium (W_{out}) is converted into potential energy by the bending of the cantilever during sample expansion. As the medium cools down and contracts, the cantilever fully returns the stored potential energy in the form of compression work (W_{in}) performed on the sample. If the tip maintains contact with the sample throughout the cycle, stroke 2 – 1 is the exact reverse of 1 – 2 and total work output ($W_{tot} = W_{out} - W_{in}$) from the engine is null when the cantilever has returned to its resting position. Such cycle provides zero efficiency and negates the usefulness of this mechanism as a classical heat engine. Nonetheless, deflection of the cantilever takes place, and provides an AFM-IR signal, even in the absence of net work output. Chopping the light beam at low frequency provides a periodical plot of deflection versus time, as schematically shown in Figure 3B, in agreement with the response observed in the first demonstration of the AFM-IR principle. [1]

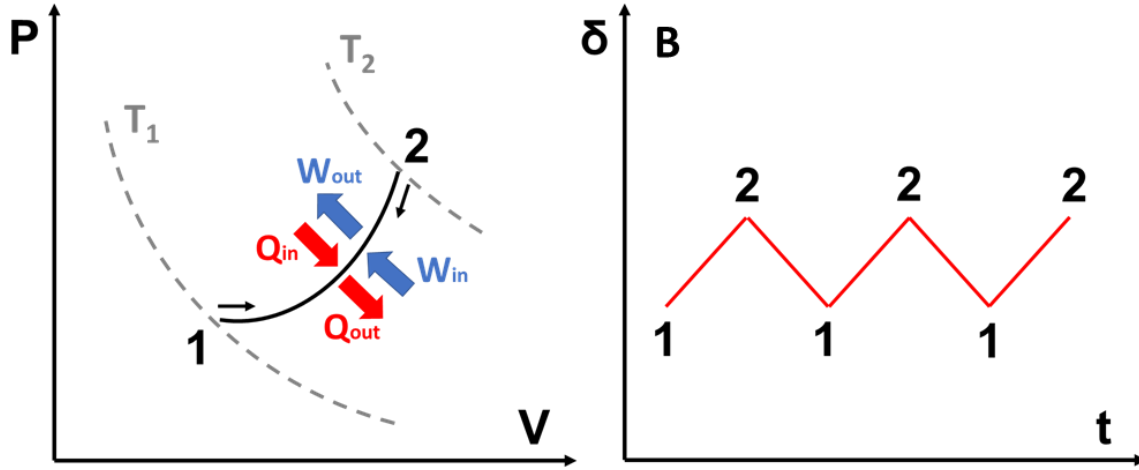


Figure 3. Continuous wave irradiation with a chopped beam. A. Corresponding engine cycle in a PV diagram. The medium absorbs light, progressing from state 1 to state 2, with a corresponding increase in pressure, volume, and temperature. Interruption of illumination leads to the thermalization and decompression of the sample, returning to state 1 by reversing the expansion stroke. **B.** Deflection corresponding to the cyclical repetition of the two strokes in panel A.

This simple model is amenable to a quantitative treatment, based on the theory of elasticity and the formalism describing the response of a solid to restricted thermal expansion, as described in the Supporting Information section. The resulting equations highlight the main quantities that affect deflection and the AFM-IR signal for a given temperature increase. The change in temperature is assumed small, so that the change in thermomechanical properties is negligible. In the simplest case, the tip of the probe can be approximated by a cylinder providing a flat contact, extending the analogy with the pistons of classical heat engines. The AFM-IR signal, as provided by the maximum deflection value, δ_{\max} , is given by Equation (1).

$$\delta_{\max} = (E^*_T \alpha_T \Delta T A)/K \quad (1)$$

E^*_T is the reduced Young modulus for the working medium and tip material at temperature T . α_T is the thermal expansion coefficient of the sample at temperature T . ΔT is the maximum temperature excursion, i.e., the temperature difference between the two isotherms ($\Delta T = T_2 - T_1$). A is the contact area between tip and sample, taken to correspond to the base of the cylindrical tip.

For the more general case of an expanding solid medium pressing against an axisymmetric tip (see Supp. Info.), the formally equivalent Equation 2 applies.

$$\delta_{\max} = E^* \alpha \Delta T \pi r^2 / K \quad (2)$$

πr^2 represents the contact surface of tip and medium and can be expressed as a function of the applied force, F_{set} (force setpoint) by using Hertz's model for indentation (see Supp. Info.), as shown in Equation 3.

$$r^2 = F_{\text{set}}^{2/3} D^{2/3} / (1/R + 1/R')^{2/3} \quad (3)$$

Where $D = \frac{3}{4} ((1-\sigma^2)/E + (1-\sigma'^2)/E')$. σ and σ' are the Poisson ratios for the working medium and for the tip respectively. E and E' are the Young moduli of the sample and of the tip respectively. R and R' are the radii of the sample surface and the tip.

Equations 1-3 express the dependence of δ_{\max} from the mechanical properties of the working medium. Larger deflection is expected from more rigid samples and from samples with larger thermal expansion coefficients, given the same temperature excursion. A small increase in deflection is also expected when operating with higher force set-point values and when using softer tips with a larger radius.

Equations 1-3 imply a dependence from the thermal properties of the medium and the environment, which is implicit in ΔT . The dependence of ΔT from the intensity of illumination and from the absorbance of the sample at the excitation wavelength(s) is the basis of the spectroscopic application of the photothermal effect and has been discussed elsewhere.[15] In addition, the value of ΔT is dependent on the thermal contact of the system with its surroundings, which determines the rate at which absorbed energy is lost to the environment as heat. For the case of gradual excitation, discussed in the present analysis, ΔT increases linearly over time when the sample is irradiated at constant power, as reported experimentally [1] and schematically represented in Figure 2B. Increasing irradiation time is eventually expected to lead to a thermal steady state, as ΔT plateaus to a stable value (not shown), which is determined by thermal exchanges between the medium and the environment.

Calculations by Morozovska *et al.* show the role of thermal conduction at the interface between different materials in determining the interplay between expansion and resolution for the case of AFM-IR with sinusoidal excitation. [11] Heat transfer processes have also been proposed to be at the basis of signal intensity and spatial resolution for the case of resonant impulsive excitation, although no calculations have been provided in support. [2] Also for the case of gradual excitation, the availability of channels for rapid thermalization implies lower expansion, lower δ_{\max} and lower AFM-IR signal. Inversely, increased deflection can be ensured by limiting heat transfer between the expanding volume and the environment.

One channel for heat dissipation which deserves attention is the tip-sample contact. Heat conduction along the AFM cantilever is used in scanning thermal microscopy, [16] and in photothermal cantilever deflection spectroscopy, [17] proving that this is a viable channel for thermal relaxation of the medium. Its contribution is expected to be relevant in the case of thick samples with low thermal conductivity, where the only other channels for thermal relaxation are the bulk of the sample itself and the surrounding air.

2.2.1 The Photothermal Engine as an Information Producing Mechanism

The quantities that are normally used to characterize the performance of classical engines, such as total work output and efficiency, appear to have no direct bearing on the performance of the AFM-IR measurement under gradual excitation, in the sense that they do not directly relate to deflection and to the intensity of the signal. The AFM-IR engine has a fundamentally different purpose than a conventional heat engine. In contrast to a classical engine, which aims to convert heat into mechanical work, the purpose of the photothermal engine in AFM-IR is the generation of information for analytical and spectroscopic purposes. The movement of the engine in response to the presence of an absorbing sample drives the movement of the

AFM laser beam. This is read out as a voltage difference at the laser detector that provides information on the presence or absence of an absorbing material. In this context, the mechanism demonstrated by Anderson [1] fully satisfies this condition, while at the same time failing to produce any useful work. This aspect will be the subject of a future separate analysis.

2.3 Case 2: Spring-Loaded Engine with Impulsive Excitation.

Impulsive excitation is the most common configuration in contemporary AFM-IR experiments, which rely on laser pulses of duration ranging from less than a nanosecond to a few microseconds. Impulsive expansion of the sample results in a rapid deflection of the cantilever followed by a ringdown decay pattern.[4,18] In this configuration the temperature of the sample increases rapidly, tracking the rise time of the pulse, then decreases exponentially after interruption of the pulse.[19] Because of the timescales involved, this mechanism is the least amenable to a description that relies on an equilibrium thermodynamic cycle. Nonetheless, some useful guidelines for the analysis of an impulsive excitation mechanism can be obtained from the cycles of Figure 1 and Figure 2, specifically for the case of a long pulse duration (i.e., the duration of the pulse is non negligible compared to the time required for thermalization). In the case of a long pulse, a rapid increase of the temperature of the sample is followed by an asymptotic convergence to a steady-state temperature (Figure 4A).[20] The rise time of the pulse ensures that most of the temperature increase occurs under isochoric conditions, while expansion occurs under approximately isothermal conditions, corresponding to transformations 1 - 2 and 2 - 3 of the cycle of Figure 4B. The cycle in Figure 4B can be considered as the limiting three-stroke case of the cycle in Figure 2, where thermalization occurs together with compression, instead of being a separate transformation. Heating of the medium by light absorption occurs during the isochoric process 1 – 2 and during the thermostatic expansion 2 – 3, whereas heat transfer to the environment occurs during 3 – 4.

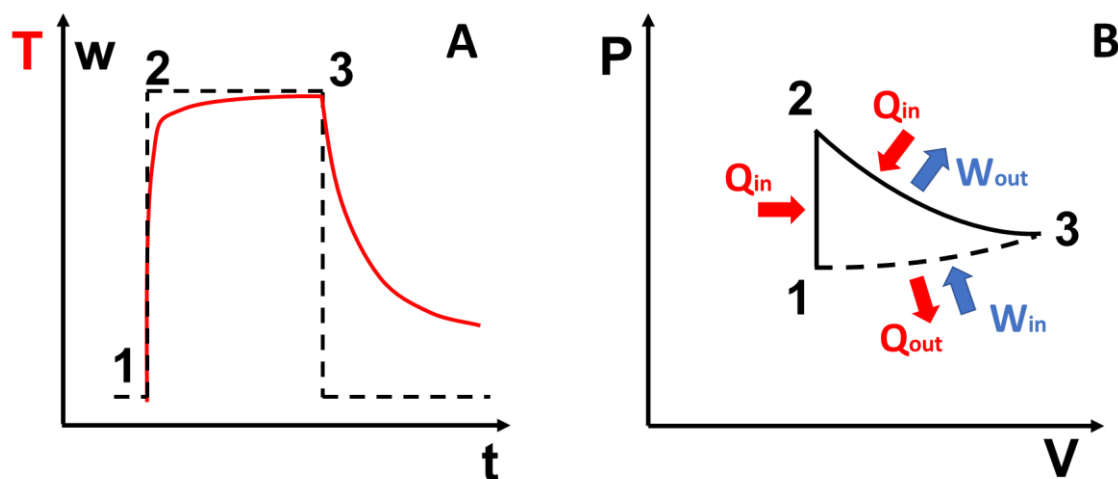


Figure 4. Impulsive excitation and its thermodynamic cycle. **A.** Pulse power (w , dotted line) and temperature increase (T , red line) within the working medium during a pulse. The temperature increases with an exponential behavior during the duration of the pulse, and decreases, also exponentially but at a different rate, after the pulse. **B.** Representation of the process in A in a PV diagram. Rapid sample heating by the pulse corresponds to an isochoric

transformation from 1 to 2. Sample expansion during pulse duration corresponds to an isothermal transformation between 2 and 3. Sample contraction during thermalization corresponds to the transformation between 3 and 1.

In contrast to the case of continuous excitation, the cycle in Figure 4B allows for non-zero values of W_{tot} and η . Resulting W_{tot} and η are expected to be small, limited by the small ΔT produced in AFM-IR experiments, typically in the range of a few degrees Kelvin. Nonetheless, the AFM-IR signal is not directly dependent on W_{tot} . In contrast, the signal can be increased by extending the duration of the isothermal stroke.

2.3.1 Work from a Spring-Loaded Engine

The possibility for an engine with a spring-loaded piston to produce useful work needs addressing. In a conventional heat engine, with a gaseous working medium, expansion increases the potential energy of the spring and compression returns this energy to the medium, providing no net work output. In contrast, the design of the photothermal engine, with a solid working medium, allows decoupling the contraction of the medium from the compression by the cantilever if the expansion/relaxation process is sufficiently rapid. It follows that part of the potential energy of the extended spring can be converted into kinetic energy of the cantilever, and later dissipated via multiple processes. This capability can be described by a *thought experiment* in Figure 5. In Figure 5A, expansion of the sample brings the cantilever to a deflected position. In contrast to the case of non-impulsive excitation, contact between the probe and the working medium is not retained throughout the cycle. We can think of a situation in which the cantilever is locked in the deflected position by some mechanism that does not consume any energy. While the medium thermalizes and contracts, the cantilever retains the stored potential energy and loses contact with the medium. After thermalization, the retention mechanism is released, and the cantilever is allowed to relax to its equilibrium position. Because of the lack of contact, the cantilever accelerates, as potential energy is converted into kinetic energy. The kinetic can be converted into usable work by coupling to an external mechanism (not represented here). If the kinetic energy is not recovered, it triggers the oscillation of the cantilever. Damping of the oscillation (Figure 5B and Figure 5C) depends on the dissipative processes at play, including inelastic collisions with the sample and friction. Synchronizing the frequency of the impulse to the frequency of a cantilever oscillation allows resonant energy transfer [7], leading to sustained sinusoidal oscillations (Figure 5D). In the latter case, signal intensity displays a complex dependence from the time structure of the pulses and from the thermal relaxation of the sample, which has already been discussed elsewhere. [2]

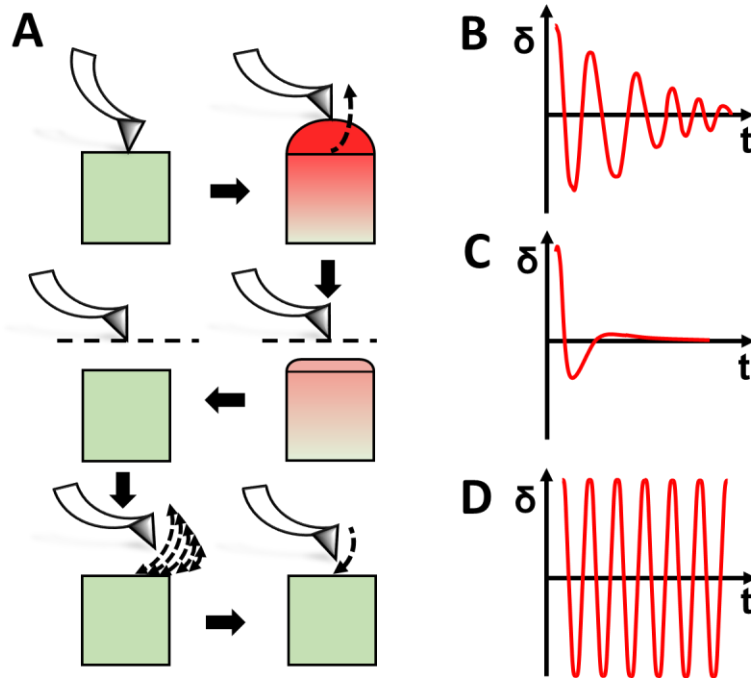


Figure 5. Probe dynamics with impulsive excitation. **A.** Expansion of the medium deflects the cantilever, leading to loss of contact between the two. The medium thermalizes and contracts while the cantilever is retained. Release of the cantilever converts its potential energy into kinetic energy, triggering its oscillation. **B.** Deflection of a lightly damped cantilever oscillation. **C.** Deflection of a highly damped cantilever oscillation. **D.** Deflection of the cantilever in resonant mode operation.

2.3.2 Tip-sample Contact During Impulsive Excitation

The analysis in Figure 5 implies loss of contact between the probe and the working medium. It has been previously assumed that in impulsive AFM-IR experiments the probe retains contact with the sample during oscillation and only contact resonances of the cantilever are excited. [6] However, this assumption has never been verified. In contrast, the present discussion argues that the tip must be displaced from the sample and excitation of non-contact resonance modes of the cantilever must take place following the initial momentum transfer. Acoustic waves of photothermal origin, as suggested by O’Callahan *et al.* [21], could also contribute to the displacement. Excitation of contact resonance modes can develop following energy transfer from non-contact modes, similarly to cantilever dynamics in multifrequency AFM experiments. [22]

Displacement of the tip from the surface has important consequences, which are neglected in theoretical treatments postulating continued contact, where excitation is limited to contact modes of the cantilever.[6] If excitation is extended to non-contact modes, the distance between tip and sample deviates from zero over time, and additional forces from tip-sample interactions can constrain cantilever deflection, affect damping, and contribute to the overall signal. Contributions to the total force can come from photoinduced forces [23], and electrostatic [24] and magnetic interactions.[25] The relative contribution of van der Waals forces [26] and of forces from photoacoustic expansion [21] would also change as a function of tip-sample distance. A quantitative treatment of the signal requires identifying and

factoring in these contributions and will not be attempted in the present section, which will focus on purely qualitative considerations.

2.3.3 Signal with Impulsive Excitation a Discussion

The AFM-IR signal with impulsive excitation is given by the maximum deflection of the cantilever, δ_{\max} , as in the case of gradual oscillation, or by the intensity of individual resonances in the resonance spectrum of the cantilever. The amplitude of the oscillations (δ_{\max}), and the total energy stored by the cantilever, is a function of the total work performed on the cantilever, in turn dependent on the duration of the pulse. Energy is accumulated in the oscillating cantilever as the combination of potential (U) and kinetic (T) energy of the oscillation. In the case of a harmonic oscillator, this is given by Equation 4, where m is the mass of the oscillator (approximated by the point mass of the cantilever/tip system positioned at its center of mass), ω_0 its normal frequency, δ_{\max} the amplitude of the oscillation, and K the force constant.

$$U + T = \frac{1}{2} m \omega_0^2 \delta_{\max}^2 = \frac{1}{2} K \delta_{\max}^2 \quad (4)$$

Equation 4 constitutes the trivial description of the energy of a harmonic oscillator. Nonetheless it affords the basic indication that increasing the amount of energy transferred to the oscillator, in the absence of dissipative processes, increases the amplitude of the oscillation. Existing descriptions of energy transfer to an oscillating cantilever have been based on Euler-Bernoulli beam theory and focused on resonant AFM-IR operation.[9,10] While these results can successfully reproduce the frequency dependence of the transfer function of the cantilever, they cannot account in a quantitative way for the efficiency of energy transfer to the oscillating cantilever, suggesting that additional analysis is required.

The mechanics of impulsive energy transfer to the cantilever are beyond the scope of this discussion, which will instead focus on the thermodynamic arguments of the previous sections. Equation 16 highlights that, in principle, any factors that improve energy transfer to the oscillating cantilever are also expected to increase the amplitude of the AFM-IR signal. Therefore, from a qualitative point of view, some of the same performance factors that maximize δ_{\max} in the case of gradual excitation can also be extended to the case of impulsive excitation.

The role of the probe as a channel for heat transmission is particularly relevant for the case of impulsive excitation, because it allows rapid heat transfer from the sample at defined time points. The periodical tip-sample contact provided by an oscillating probe can define the duration of thermostatic expansion stages and allow for rapid thermalization in synchrony with the oscillation of the cantilever. In cases where the laser pulse induces direct heating of the cantilever, the contact may also act as a timed heat source towards the sample, modulating its excitation.[27] Synchronization of the contact with excitation pulses can provide increased deflection by allowing a longer thermostatic expansion stroke. This condition has indeed been realized in a micromechanical heat engine with a periodical cantilevered contact to a heat source and heat sink.[28] In this context, resonant AFM-IR operation provides fine synchronization of laser pulses with the cantilever oscillation, thus providing optimal conditions for heat exchange between the sample and the tip. In agreement with the present analysis, it has been shown by Lu *et al.* that resonant operation provides thermostatic conditions in the measurement of thin films.[29] The timing of excitation and

heat relaxation may be a contributing factor to the signal observed in resonant mode excitation and to the dependence of the resonant signal from the frequency and pulse length of the laser, delivering stronger signal with longer pulses.[2] Specific experiments need to be designed to quantify the contribution of the probe to heat exchange processes between sample and environment.

2.4 Testing the Photothermal Engine Model: Non-Impulsive Excitation

Testing the predictive capability of the photothermal engine model goes hand in hand with its use in the optimization of an AFM-IR experiment. The treatment provided by equations 1 - 3 is limited to the case of excitation by a continuous light source, described in Figure 3. Therefore, the discussion in this section is mostly limited to this specific case. It relies on the consideration that the intensity of the AFM-IR signal parallels the deflection of the cantilever, δ_{\max} .

It follows immediately from equations 1 - 3 that δ_{\max} increases with ΔT and with the optical parameters that affect ΔT , such as the absorption coefficient at the wavelength of excitation. This is the generally accepted dependence of the AFM-IR signal from the macroscopic absorption spectrum of the sample, which is the basis of the spectroscopic and analytical applications of the technique. Equations 1 - 3 also define the dependence of the signal from the thermomechanical properties of the system. Intuitively, materials with larger thermal expansion α deliver stronger signal. Stiffer materials, with larger values of E , deliver stronger signal. Maximum deflection and signal also decrease with increasing K , showing that softer cantilevers provide higher sensitivity. Some of these conclusions have also been reached by the analysis performed by Lu *et al.* [29]. In contrast, the dependence from K is opposite to the one predicted by Dazzi *et al.* [6], according to which the signal increases proportionately with stiffness.

Equations 1 - 3 also highlight a proportional relationship between the AFM-IR signal and the contact surface between tip and sample. In line with our thermodynamic analysis, this dependence bears some analogy to the role of the compression ratio on the performance of internal combustion engines. The effect of the tip-sample contact area may be contributing to the difference in signal intensity that we reported when measuring convex and concave sample surfaces.[15] While Equations 2 and 3 were derived for two specific geometries, the power dependence between contact surface and force is the same for all geometries, [30] and the proportionality between δ_{\max} and contact area will be retained for any sample and tip geometry.

We can test the validity of Equation 2 by comparing its predictions for a real sample. Let us consider a sample of polystyrene (PS), for which $E = 3 \times 10^9$ Pa and a the linear thermal expansion coefficient $\alpha = 7 \times 10^{-5} K^{-1}$. [31] We irradiate the sample with light at the frequency of the absorption bands of PS, producing a $\Delta T = 1$ K, a reasonable value for the T increase in a polymer sample irradiated with a light source of a few 100's μW (such as from a thermal source for FTIR spectroscopy or a laser). [15] We monitor its expansion using a contact mode AFM probe with $K = 1$ N/m and $r = 50$ nm. Equation 2 provides a value of maximum deflection $\delta_{\max} = 1.6$ nm, close to the value of 1.5 nm reported by Anderson. While this is only an approximate verification, it shows that Equation 2 produces values that are in the range of available experimental results.

While the tip-sample contact geometry is well known to affect contact micromechanics in AFM applications, it has received little attention in AFM-IR applications. Existing theoretical treatments of AFM-IR either neglect the role of tip-sample contact [11] or limit the discussion to the effect of the contact on the resonant frequency of the cantilever.[9][10][6] Only the analysis by Dazzi *et al.* [6] and the one by Lu *et al.* [29] explicitly consider the dependence of the force from the contact surface, although the former provides a lower dimensional dependence. The present treatment confirms that increasing the contact surface delivers a proportionally higher force and deflection, thus increasing the AFM-IR signal, in a trade-off with spatial resolution. Increasing the force applied to a spherical tip is also expected to provide higher signal because of the resulting increase in contact area. Additionally, it is expected that all factors that influence the mechanics of tip-sample contact, such as adhesion forces and tip geometry also affect deflection and AFM-IR signal. These factors have been described by the various quantitative treatments of contact mechanics from the AFM community [32] and will not be addressed in detail in the present work. One final observation is that while the geometry of the tip-sample contact has direct bearing on the mechanics of the expansion, it can also play a role in the thermal relaxation of the sample, acting as a channel for heat conduction. Targeted experiments are necessary to clarify this aspect.

The conclusions from this discussion are summarized in Table I, which shows the expected effect of some parameters on the intensity of the AMF-IR signal. The entries in Table I include all the quantities used for Equations 1 – 3 and can be used both as guideline for the optimization of AMF-IR experiments and as a reference to test the model described in this work.

Table I. Effect on Sample and Probe parameters on the AFM-IR signal. *K*: Cantilever Force Constant. *A*: Tip/Sample contact surface. *E*, *E'*: Young Moduli of Sample and Tip. α : Thermal Expansion Coefficient of Sample. σ , σ' : Poisson Ratios of Tip and Sample. F_{set} : Force Setpoint. *R*, *R'*: Radii of Tip and Sample Surface. ΔT : Photothermal Induced Temperature Increase.

Parameter	Expected Correlation with Signal Intensity
K	-
A	+
E	+
E'	-
α	+
σ, σ'	-
F_{set}	+
R, R'	+
ΔT	+

2.5 Testing the Photothermal Engine Model: Impulsive Excitation

The displacement of the tip from the surface increases the complexity of the analysis for the case of impulsive excitation and limits our capability to define parameters for optimization of the signal. Upon loss of contact, photoinduced forces [23] acting between tip and sample can constrain the deflection of the cantilever, effectively decreasing the AFM-IR signal. In addition, all forces affecting the interaction between tip and sample, including Van der Waals [26], electrostatic [33], and adhesion forces [26] need to be factored in when assessing the response of the cantilever as the tip-sample distance is changed. The decay of the cantilever oscillation is also conditional to the action of such forces. Some of these interactions increase in magnitude with the area of the tip-sample contact and can complement or offset the mechanical advantage provided by a larger contact area. In the case of two-material layered cantilevers, heat transmission from the heated medium [17] or direct absorption of the excitation laser light [27] can provide additional contributions to deflection, further complicating the description. Therefore, the simple guidelines obtained for the case of gradual excitation cannot be immediately extended to the case of impulsive excitation. The multiplicity of these interactions, their overlapping contributions, and the influence of environmental factors on their magnitude (e.g., the effect of humidity on capillary and electrostatic forces) provide a future challenge for the modelling of AFM-IR signal intensity in the case of pulsed excitation. First and foremost, it is imperative to assess experimentally whether contact between sample and tip is lost during impulsive excitation, to define the contour conditions for any theoretical description.

3.0 Conclusions

In this work we have described the detection scheme of the AFM-IR experiment in terms of a light-driven micromechanical engine. Much of the treatment and discussion is based on AFM-IR operation relying on gradual excitation by a continuous light source. We assume that the displacement of the AFM probe is determined exclusively by photothermal expansion and propose a thermodynamic engine cycle as a framework to analyze the properties of such mechanism. Our preliminary analysis highlights the main quantities that can affect the performance of the engine and of the associated AFM-IR experiment, including the area of the tip-sample contact, the thermoelastic properties of tip and sample, and the nature of channels for heat dissipation. Therefore, from the perspective of an AFM-IR experiment, the engine can be optimized for signal generation, and we provide practical guidelines to this purpose.

We also comment on the possibility to extend a thermodynamic engine analysis to the case of impulsive excitation. In such case, tip displacement from the sample surface introduces additional contributions from multiple interactions between tip and sample which greatly increase the complexity of the analysis and limit our capability to develop a theoretical treatment. Indeed, we propose that AFM-IR experiments with continuous and with impulsive excitation are fundamentally different, and only the former relies predominantly on measurement of the photothermal effect, while the latter is responsive to a multitude of additional interactions.

A thermodynamic analysis can also guide the design of new instrumental configurations, which depart from the conventional scheme based on cantilever deflection. In a more general sense, the model presented in this work can account for the diverse facets of the photothermal

micromechanical detection scheme, including optical, and thermodynamic aspects in one single description.

A detailed understanding of the nature of heat reservoirs and heat exchange will be relevant for the optimization of photothermal measurements in fluids, such as water. To date experiments in an aqueous environment have been analyzed only in terms of mechanical factors, such as the damping of cantilever oscillations in a fluid. However, the heat capacity and thermal conductivity of the aqueous environment are also important, and so far neglected, factors in determining AFM-IR signal generation.

The present discussion is based on classical thermodynamics and is valid as long as samples can be described by their bulk properties. This is a common regime for AFM-IR samples, which in most cases are thicker than 100 nm. However, AFM-IR experiments also extend to samples 10 nm or less in size, particularly when resonant mode excitation is used, which provides signals from samples as thin as a molecular monolayer. Such measurements straddle into the realm of single molecule physics and of quantum mechanics and need models different than the macroscopic ones provided here for a satisfactory description.

Funding

This work was supported by an OPUS16 grant from the National Science Centre Poland [contract 2018/31/B/NZ1/01345].

References

- [1] M.S. Anderson, Infrared spectroscopy with an atomic force microscope, *Appl. Spectrosc.* 54 (2000) 349–352. <https://doi.org/10.1366/0003702001949618>.
- [2] L. Quaroni, Understanding and Controlling Spatial Resolution, Sensitivity, and Surface Selectivity in Resonant-Mode Photothermal-Induced Resonance Spectroscopy, *Anal. Chem.* 92 (2020) 3544–3554. <https://doi.org/10.1021/acs.analchem.9b03468>.
- [3] L. Quaroni, Infrared microscopy in the study of cellular biochemistry, *Infrared Phys. Technol.* 105 (2020) 102779. <https://doi.org/10.1016/j.infrared.2018.11.026>.
- [4] A. Dazzi, R. Prazeres, F. Glotin, J.M. Ortega, Local infrared microspectroscopy with subwavelength spatial resolution with an atomic force microscope tip used as a photothermal sensor, *Opt. Lett.* 30 (2005) 2388–2390. <https://doi.org/10.1364/OL.30.002388>.
- [5] A. Dazzi, PhotoThermal Induced Resonance. Application to Infrared Spectromicroscopy, in: S. Volz (Ed.), *Therm. Nanosyst. Nanomater.*, Springer, Berlin, 2009: pp. 469–503.
- [6] A. Dazzi, F. Glotin, R. Carminati, Theory of infrared nanospectroscopy by photothermal induced resonance, *J. Appl. Phys.* 107 (2010) 124519. <https://doi.org/10.1063/1.3429214>.
- [7] F. Lu, M.A. Belkin, Infrared absorption nano-spectroscopy using sample photoexpansion induced by tunable quantum cascade lasers., *Opt. Express.* 19 (2011) 19942–7. <https://doi.org/10.1364/OE.19.019942>.
- [8] D.E. Barlow, J.C. Biffinger, A.L. Cockrell-Zugell, M. Lo, K. Kjoller, D. Cook, W.K. Lee, P.E. Pehrsson, W.J. Crookes-Goodson, C.S. Hung, L.J. Nadeau, J.N. Russell, The importance of correcting for variable probe-sample interactions in AFM-IR spectroscopy: AFM-IR of dried bacteria on a polyurethane film, *Analyst.* 141 (2016)

- 4848–4854. <https://doi.org/10.1039/c6an00940a>.
- [9] G. Ramer, F. Reisenbauer, B. Steindl, W. Tomischko, B. Lendl, Implementation of Resonance Tracking for Assuring Reliability in Resonance Enhanced Photothermal Infrared Spectroscopy and Imaging, *Appl. Spectrosc.* 71 (2017) 2013–2020. <https://doi.org/10.1177/0003702817695290>.
- [10] S. Kenkel, A. Mittal, S. Mittal, R. Bhargava, Probe-Sample Interaction-Independent Atomic Force Microscopy-Infrared Spectroscopy: Toward Robust Nanoscale Compositional Mapping, *Anal. Chem.* 90 (2018) 8845–8855. <https://doi.org/10.1021/acs.analchem.8b00823>.
- [11] A.N. Morozovska, E.A. Eliseev, N. Borodinov, O.S. Ovchinnikova, N. V. Morozovsky, S. V. Kalinin, Photothermoelastic contrast in nanoscale infrared spectroscopy, *Appl. Phys. Lett.* 112 (2018) 033105. <https://doi.org/10.1063/1.4985584>.
- [12] C. Mayet, A. Dazzi, R. Prazeres, J.-M. Ortega, D. Jaillard, In situ identification and imaging of bacterial polymer nanogranules by infrared nanospectroscopy, *Analyst.* 135 (2010) 2540. <https://doi.org/10.1039/c0an00290a>.
- [13] A. Hammiche, L. Bozec, H.M. Pollock, M. German, M. Reading, Progress in near-field photothermal infra-red microspectroscopy, *J. Microsc.* 213 (2004) 129–134. <https://doi.org/10.1111/j.1365-2818.2004.01292.x>.
- [14] P.M. Donaldson, C.S. Kelley, M.D. Frogley, J. Filik, K. Wehbe, G. Cinque, Broadband near-field infrared spectromicroscopy using photothermal probes and synchrotron radiation, *Opt. Express.* 24 (2016) 1852. <https://doi.org/10.1364/OE.24.001852>.
- [15] L. Quaroni, Imaging and spectroscopy of domains of the cellular membrane by photothermal-induced resonance, *Analyst.* 145 (2020) 5940–5950. <https://doi.org/10.1039/d0an00696c>.
- [16] M. Nonnenmacher, H.K. Wickramasinghe, Scanning probe microscopy of thermal conductivity and subsurface properties, *Appl. Phys. Lett.* 61 (1992) 168–170. <https://doi.org/10.1063/1.108207>.
- [17] S. Kim, D. Lee, T. Thundat, Photothermal Cantilever Deflection Spectroscopy, *EPJ Tech. Instrum.* (2014) 7. <https://doi.org/10.1140/epjti/s40485-014-0007-1>.
- [18] A.M. Katzenmeyer, G. Holland, K. Kjoller, A. Centrone, Absorption Spectroscopy and Imaging from the Visible through Mid-Infrared with 20 nm Resolution, *Anal. Chem.* 87 (2015) 3154–3159. <https://doi.org/10.1021/ac504672t>.
- [19] A.M. Katzenmeyer, G. Holland, J. Chae, A. Band, K. Kjoller, A. Centrone, Mid-infrared spectroscopy beyond the diffraction limit via direct measurement of the photothermal effect, *Nanoscale.* 7 (2015) 17637–17641. <https://doi.org/10.1039/c5nr04854k>.
- [20] V.P. Zharov, V.S. Letokhov, *Laser Optoacoustic Spectroscopy*, Springer Berlin Heidelberg, Berlin, Heidelberg, 1986.
- [21] B.T. O’Callahan, J. Yan, F. Menges, E.A. Muller, M.B. Raschke, Photoinduced Tip-Sample Forces for Chemical Nanoimaging and Spectroscopy, *Nano Lett.* 18 (2018) 5499–5505. <https://doi.org/10.1021/acs.nanolett.8b01899>.
- [22] R. Garcia, E.T. Herruzo, The emergence of multifrequency force microscopy, *Nat. Nanotechnol.* 7 (2012) 217–226. <https://doi.org/10.1038/nnano.2012.38>.
- [23] D. Nowak, W. Morrison, H.K. Wickramasinghe, J. Jahng, E. Potma, L. Wan, R. Ruiz, T.R. Albrecht, K. Schmidt, J. Frommer, D.P. Sanders, S. Park, Nanoscale chemical imaging by photoinduced force microscopy, *Sci. Adv.* 2 (2016). <https://doi.org/10.1126/sciadv.1501571>.
- [24] J.E. Stern, B.D. Terris, H.J. Mamin, D. Rugar, Deposition and imaging of localized charge on insulator surfaces using a force microscope, *Appl. Phys. Lett.* 53 (1988)

- 2717–2719. <https://doi.org/10.1063/1.100162>.
- [25] Y. Martin, H.K. Wickramasinghe, Magnetic imaging by “force microscopy” with 1000 Å resolution, *Appl. Phys. Lett.* 50 (1987) 1455–1457. <https://doi.org/10.1063/1.97800>.
- [26] A.L. Weisenhorn, P.K. Hansma, T.R. Albrecht, C.F. Quate, Forces in atomic force microscopy in air and water, *Appl. Phys. Lett.* 54 (1989) 2651–2653. <https://doi.org/10.1063/1.101024>.
- [27] B. Kwon, M. Rosenberger, R. Bhargava, D.G. Cahill, W.P. King, Dynamic thermomechanical response of bimaterial microcantilevers to periodic heating by infrared radiation, *Rev. Sci. Instrum.* 83 (2012) 015003. <https://doi.org/10.1063/1.3680107>.
- [28] L.W. Weiss, J.H. Cho, K.E. McNeil, C.D. Richards, D.F. Bahr, R.F. Richards, Characterization of a dynamic micro heat engine with integrated thermal switch, *J. Micromechanics Microengineering.* 16 (2006) S262–S269. <https://doi.org/10.1088/0960-1317/16/9/S14>.
- [29] F. Lu, M. Jin, M.A. Belkin, Tip-enhanced infrared nanospectroscopy via molecular expansion force detection, *Nat. Photonics.* 8 (2014) 307–312. <https://doi.org/10.1038/nphoton.2013.373>.
- [30] L.D. Landau, E.M. Lifshitz, *Theory of Elasticity*, 2nd Ed., Pergamom Press, Oxford, 1970.
- [31] J.E. Mark (Editor), *Physical Properties of Polymers Handbook*, Second Ed., Springer, 2007.
- [32] R. Garcia, Nanomechanical mapping of soft materials with the atomic force microscope: Methods, theory and applications, *Chem. Soc. Rev.* 49 (2020) 5850–5884. <https://doi.org/10.1039/d0cs00318b>.
- [33] B.D. Terris, J.E. Stern, D. Rugar, H.J. Mamin, Localized charge force microscopy, *J. Vac. Sci. Technol. A Vacuum, Surfaces, Film.* 8 (1990) 374–377. <https://doi.org/10.1116/1.576399>.

Supporting Information for “Analysis of the Photothermal Engine Cycle in an AFM-IR Measurement of Photothermal Expansion”

Luca Quaroni

Department of Physical Chemistry and Electrochemistry, Faculty of Chemistry, Jagiellonian University, 30-387, Kraków, Poland.

Index of Contents

Page 20	Index of Contents
Page 21	Cantilever Deflection in a Photothermal Engine
Page 22	References

Cantilever Deflection in a Photothermal Engine

Flat piston engine

Maximizing the AFM-IR signal corresponds to maximizing the deflection (δ) of the cantilever of the AFM probe. The sensitivity of the response is determined by the deflection produced by a unit temperature increase in the sample. In turn, the maximum deflection is determined by balancing the force associated to the expansion of the working medium, F_e , with the force exerted by the cantilever, F_c . F_e is calculated as the force exerted by a compressible medium undergoing constrained expansion. For a probe with a cylindrical tip, F_e is given by Equation s1.

$$F_e = E_T^* \alpha_T \Delta T A \quad (s1)$$

E_T^* is the reduced Young modulus for the working medium at temperature T . If the Young modulus for the cantilever is much larger than that for the sample (a common case when using conventional AFM tips of silicon or silicon nitride with soft samples), then E_T^* approximates to E_T for the sample. α_T is the thermal expansion coefficient of the sample at temperature T . ΔT is the temperature difference between the two isotherms of operation ($\Delta T = T_2 - T_1$). A is the contact area between tip and sample. A is equivalent to the area of the base of the cylindrical tip within the assumption that the sample is larger than the tip. Equation s1 assumes a small compression, such that shear stress at the edges of the compression area is negligible.

The deflection of the cantilever, δ , under the action of this force, is given by Hook's Law in the case of harmonic behavior (Equation s2).

$$F_c = - \delta K \quad (s2)$$

K is the spring constant for the cantilever. The maximum deflection, δ_{\max} , caused by a given temperature increase ΔT is obtained when $F_e = - F_c$ and is given by Equation s3.

$$\delta_{\max} = (E_T \alpha_T \Delta T A)/K \quad (s3)$$

General Case: two contacting spheres with an external applied force

For applications of the engine to nanoscale spectroscopy, the driving force in AFM-IR development, a more general description is useful. The tip-sample interaction force is better described by models that account for the specific geometry of the tip and the sample. The force exerted on a spherical tip by the expanding spherical sample, the most common geometry in AFM-IR applications, has already been described.¹ By using this formalism we can relate the contact area of two bodies compressed by an external force to their mechanical and geometrical properties and the acting force. In analogy with the previous case, we can write Equation s4.

$$F_e = E \alpha \Delta T \pi r^2 \quad (s4)$$

Where πr^2 is the contact surface between the two compressed elastic spherical bodies.

According to Landau and Lifshitz (Chapter 9)¹, it can be shown that r^2 is a function of the mechanical and geometrical properties of tip and sample and of the applied external force, following Equation s5.

$$r^2 = F_{\text{set}}^{2/3} D^{2/3} / (1/R + 1/R')^{2/3} \quad (\text{s5})$$

R and R' are the radii of the sample surface and of the tip. F_{set} is the force setpoint. D is given by Equation s6.

$$D = \frac{3}{4} \left((1-\sigma^2)/E + (1-\sigma'^2)/E' \right) \quad (\text{s6})$$

σ and σ' are the Poisson ratios for the working medium and for the tip respectively. E and E' are the Young moduli of the sample and of the tip respectively.

If the curvature of the sample is negligible compared to the curvature of the tip, Equation s5 reduces to Equation s7.

$$r^2 = (F_{\text{set}} D R')^{2/3} \quad (\text{s7})$$

If the modulus of the sample is much lower than the modulus of the tip (the common case of a hard tip and a soft sample), Equation s6 reduces to Equation s8.

$$D = \frac{3}{4} (1-\sigma^2)/E \quad (\text{s8})$$

The maximum deflection is then given by Equation s9

$$\delta_{\text{max}} = E \alpha \Delta T \pi r^2 / K \quad (\text{s9})$$

References for Supporting Information

- 1 L. D. Landau and E. M. Lifshitz, *Theory of Elasticity*, Pergamon Press, Oxford, 2nd Edition, 1970.